Available online at www.sciencedirect.com
SCIENCE DIRECT®
Journal of Power Sources 117 (2003) 242–248
JOURNAL OF POWER SOURCES
www.elsevier.com/locate/jpowsour

Galvanostatic non-destructive characterization of alkaline silver–zinc cells

B. Hariprakash, S.K. Martha, A.K. Shukla*

Solid State and Structural Chemistry Unit, Indian Institute of Science, Bangalore 560012, India

Received 9 December 2002; accepted 24 January 2003

Abstract

Alkaline silver–zinc cells of different capacity have been characterised by a galvanostatic non-destructive technique (GNDT). Cells with capacities between 10.6 and 58.5 Ah exhibit lower internal resistance than those with capacities between 1.7 and 5.8 Ah. From analysis of voltage–time transient data, it is concluded that only the cells with capacities between 10.6 and 58.5 Ah can sustain high-drain applications.

Keywords: Alkaline silver–zinc batteries; Galvanostatic non-destructive characterization; Faradaic efficiency; Capacity; Internal resistance; High-drain applications

1. Introduction

Alkaline silver–zinc batteries are used in a variety of aerospace and military applications due to their high specific and volumetric energy densities [1–3]. These batteries are produced commercially with a wide range of nominal capacities. In recent years, several improvements have been made to the batteries, which include [4–18]; (i) new separator materials as alternatives to the conventional membranes; (ii) improved zinc electrodes with additives to mitigate shape change and dendritic growth; (iii) additives to the electrolyte to reduce zinc dissolution in the electrolyte; and (iv) improved processing of silver active material.

The impedance of silver–zinc cells is normally low, but can vary considerably with factors such as discharge current density, state-of-charge (SoC), charge stand, cells ageing, operational temperature, separator material and more importantly, cell size [19]. Interestingly, only a few studies on the impedance of silver–zinc batteries have been reported [2,20].

As a part of an ongoing research programme on the characterization of secondary batteries by means of a galvanostatic non-destructive technique (GNDT) [21–23], a study is made of alkaline silver–zinc cells of different capacity.

2. Experimental

Silver–zinc (Ag–Zn) cells of varying capacity were obtained form High Energy Batteries (India) Limited, Mathur, Tamil Nadu, in a reserve condition. The required quantity of 6 M KOH electrolyte was added and the electrodes were allowed to soak for 72 h. The cells were conditioned by conducting a few charge–discharge formation cycles. The nominal characteristics of these cells are presented in Table 1. During formation, the cells were charged at the *C*/20 rate up to 2.05 V followed by the discharge to a cut-off voltage of 1 V. Formation cycling of the cells was continued at the *C*/10 rate until the cells reached their maximum attainable capacity. Subsequently, a galvanostatic non-destructive technique was used to characterize these cells at different state-of-charge values. (Note, the SoC is the ratio of available capacity to the maximum attainable capacity.)

The cells were fully charged and kept at open circuit for about 30 min to allow the open-circuit voltage to stabilize. The cells were then discharged galvanostatically at the *C*/5 rate for a pre-determined period so as to attain the required SoC. Subsequently, cells were again kept at open-circuit for about 30 min to attain equilibrium. The stable value of open-circuit voltage was noted and the GNDT experiments were performed. The SoC of the cells was taken as zero at 1 V. The electrical circuit employed in the present study is shown in Fig. 1. It comprised the test cells, a variable resistor, a regulated dc power supply, and a micro-switch. The technique involved discharge of the test cell at a substantially

* Corresponding author. Tel.: +91-80-3092795; fax: +91-80-3601310.
E-mail address: shukla@sscu.iisc.ernet.in (A.K. Shukla).

0378-7753/03/$ – see front matter
doi:10.1016/S0378-7753(03)00163-0

Table 1
Nominal characteristics of silver–zinc cells

Cell type	Cell capacity (Ah)	Cell height (mm)	Cell width (mm)	Cell thickness (mm)	Cell weight (g)	Cell volume (ml)	Electrolyte volume (ml)
HR1	1.7	43.70	27.60	13.90	30.206	16.765	3.5
HR3	5.8	63.85	43.80	15.85	93.131	44.326	13.5
HR5	10.6	63.95	52.70	20.25	132.599	68.246	16.0
HR10	17.2	96.25	41.45	27.75	223.240	110.710	33.0
HR15	24.5	93.20	56.80	33.05	351.060	174.959	52.0
HR40	58.5	162.0	82.60	24.20	727.000	323.825	100.0

low rate ($\sim C/450$) over a period of only about 300 s. Since the variation in cell voltage was very small under this discharge condition, it was necessary to compensate with a potential divider to obtain precise measurements.

The measurements of the compensated voltage at any instant was made with an ADC/DAC/Timer/Opto-Isolate I/O Card (Advanced Electronic Systems, Bangalore, India), which was interfaced to a PC compatible channel bus, and the data acquisition was carried out with a program written in C^{++}. The data were collected at intervals of 300 ms for a total period of 300 s. All experiments were performed at 27($\pm$1) °C. The noise level in the collected data was within $\pm$76 μV. The data were smoothened and analysed with the aid of Microcal Origin software. The fitting of the data was examined with the χ^2-test and the derived values were found to be of the order of 10^{-5} which reflect the accuracy of the fitting procedure. Data collection and analysis were carried out at several SoC values of the test cells in order to check for reproducibility.

3. Results and discussion

Silver–zinc cells were found to form within to two to three charge–discharge cycles. Typical charge–discharge curves are shown in Fig. 2. Fully-conditioned cells are found to yield a Faradaic efficiency of about 95% [14]. The equivalent circuit of the test cells under the conditions described in Section 2 is shown in Fig. 3, where T_1 and T_2 are the cells terminals, R_Ω is the ohmic resistance, $R_{t,1}$ is the charge-transfer resistance, and $C_{d,1}$ is the interfacial capacitance comprising of double-layer capacitance and the associated capacitive components due to adsorption, passive films, etc., for one of the electrodes, while $R_{t,2}$ and $C_{d,2}$ are the charge-transfer resistance and the interfacial capacitance for the other electrode.

3.1. Galvanostatic non-destructive technique

The GNDT technique monitors the state-of-health of a battery by analysing its impedance parameters [24]. (Note, the measurements reflects the state-of-health of a battery by taking into account charge-acceptance, internal resistance, voltage, and self-discharge.) Since the discharge current corresponding to $C/450$ rate is restricted to a duration of a couple of minutes only, the SoC of the test cell changes only by 10^{-5} and can be taken to be nearly invariant for all practical purposes. Accordingly, it can be assumed that the charge-transfer processes are the rate-determined steps for both the electrode reactions. Since the electrode processes

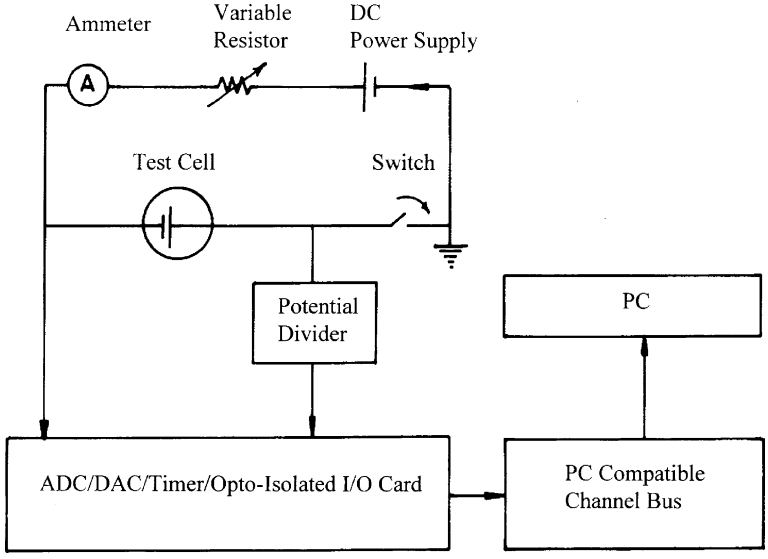

Fig. 1. Schematic of set-up for digital recording of voltage–time transients under GNDT conditions.

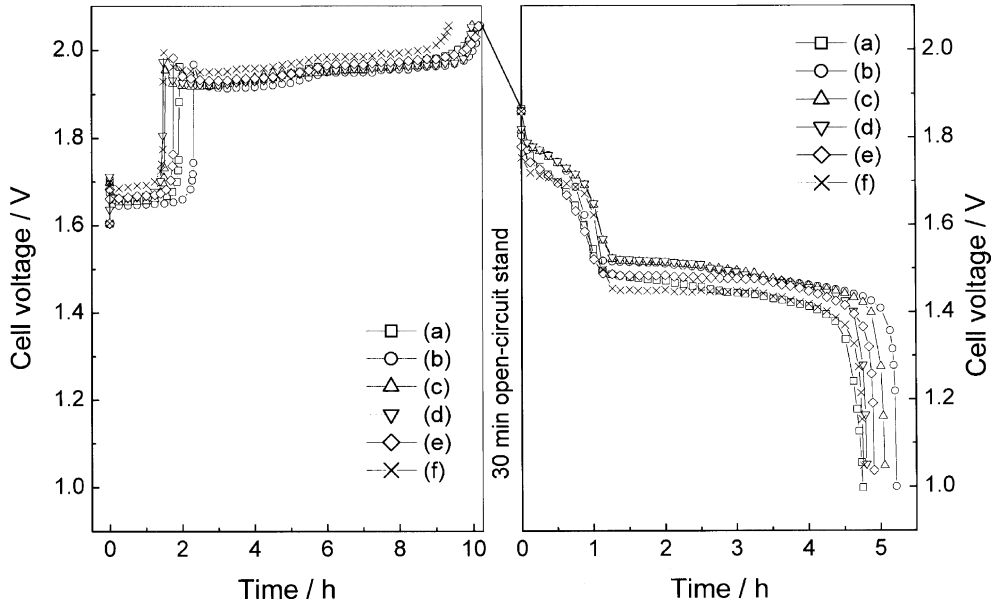

Fig. 2. Typical charge–discharge curves for silver–zinc cells of type: (a) HR1, (b) HR3, (c) HR5, (d) HR10, (e) HR15, (f) HR40.

are not governed by mass transfer, the Warburg components are not included in the equivalent circuit [24,25].

For a small current perturbation, the voltage response of the test cells can be written with reference to the equivalent circuit shown in Fig. 3 as:

$$V_r - V = IR_\Omega + IR_{t,1}\left[1 - \exp\left(\frac{-t}{\tau_1}\right)\right] + IR_{t,2}\left[1 - \exp\left(\frac{-t}{\tau_2}\right)\right] \quad (1)$$

where V_r is the voltage of the cell at rest, V the voltage of the cell at a particular time, I the discharge current, τ_1 ($=R_{t,1}C_{d,1}$) and τ_2 ($=R_{t,2}C_{d,2}$) are the time constants of the associated electrode processes. The exponential terms in Eq. (1) are due to the charging of $C_{d,1}$ and $C_{d,2}$. At time $t > \tau_1$ and, τ_2 the capacitors are completely charged and therefore the voltage drop is only due to resistive components [21–25], namely, $R_{t,1}$, $R_{t,2}$ and R_Ω.

A solution of Eq. (1) provides the impedance parameters of the cell. Since there are serious limitations in the direct algebraic procedure to solve Eq. (1), an alternative approach becomes imperative. This procedure assumes that the time constants τ_1 and τ_2 differ by one order of magnitude. The procedure involves the following steps.

Step 1: Eq. (1) shows that V versus t is non-linear. Two instances of time (t^* and t^{**}) in the initial region of the V–t curve are chosen such that there is a measurable difference in the corresponding slopes (m^* and m^{**}) of the curve. Although the time zone of these slopes is governed by the relaxation processes at both the electrodes, as an approximation, it is assigned entirely to one of the processes, i.e. the τ_1 process. The approximate value of τ_1, viz. τ_1', is given by:

$$\tau_1' = \frac{t^{**} - t^*}{\ln(-m^{*)} - \ln(-m^{**})} \quad (2)$$

which is obtained by differentiating Eq. (1) with respect to time (t) and neglecting the contribution from the τ_2 process.

Step 2: Since the function $[1 - \exp(-t/\tau)]$ attains about 99% of its final value at $t = 5\tau$, it is assumed that the relaxation at $t > 5\tau_1'$ is due only to the τ_2 process. Under this condition, Eq. (1) reduces to:

$$V_r - V = I(R_\Omega + R_{t,1}) + IR_{t,1}\left[1 - \exp\left(\frac{-t}{\tau_2}\right)\right] \quad (3)$$

on differentiating Eq. (3) with respect to time (t) yields:

$$\ln\left(\frac{-dV}{dt}\right) = \ln\left(\frac{IR_{t,2}}{t_2}\right) - \frac{t}{\tau_2} \quad (4)$$

A linear plot of $\ln(-dV/dt)$ versus t in the time domain $t > 5\tau_1'$ provides τ_2 and $R_{t,2}$ from its slope and intercept, and hence $C_{d,2}$. Substitution of Eq. (4) in Eq. (3) followed by a plot of $(V_r - V)$ versus $\exp(-t/\tau_2)$ gives a straight line in the time domain $t > 5\tau_1'$. The intercept of the plot with the y-axis gives the value of the total internal resistance, i.e. R_i ($=R_\Omega + R_{t,1} + R_{t,2}$).

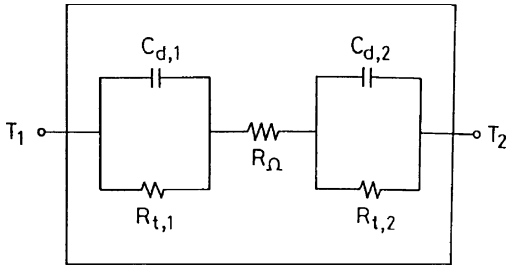

Fig. 3. Equivalent circuit for silver–zinc cells under GNDT conditions.

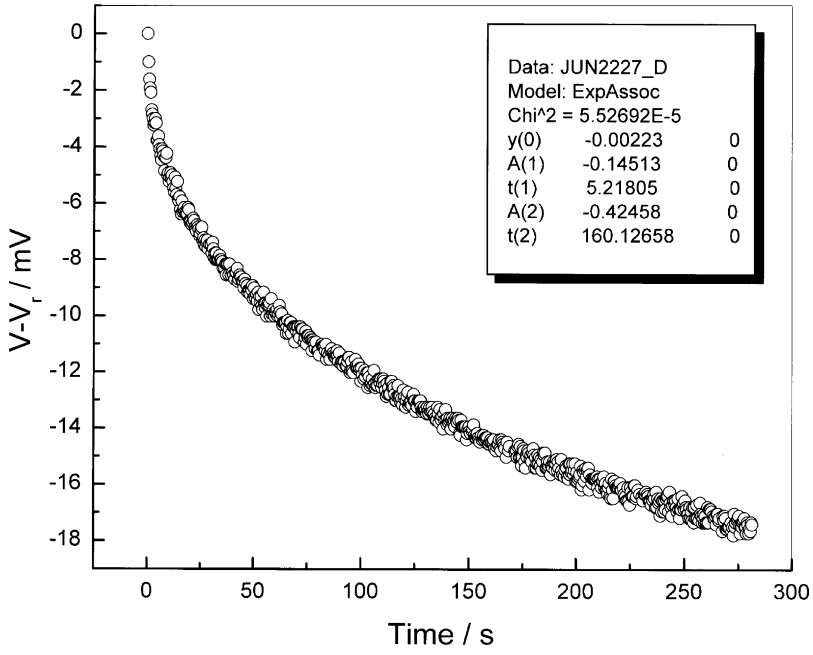

Fig. 4. Typical galvanostatic discharge transient of silver–zinc cell, type HR3, at SoC = 1.

Step 3: Eq. (1) is now recast as:

$$Y = -IR_{t,1} \exp\left(\frac{-t}{\tau_1}\right) \quad (5)$$

where $(Y = V_r - V - IR_i + IR_{t,2}) \exp(-t/\tau_2)$. Therefore,

$$\ln(-Y) = \frac{\ln(IR_{t,1}) - t}{\tau_1} \quad (6)$$

Since Y is now known completely at each values of t, a plot of $\ln(-Y)$ versus t in the time domain $t < \tau_2/5$ yields a straight line of slope $(-1/\tau_1)$ and intercept $IR_{t,1}$ This step provides the values of τ_1 and $R_{t,1}$, and hence $C_{d,1}$. Furthermore, R_Ω can also be calculated. All the five parameters, namely R_Ω, $R_{t,1}$, $R_{t,2}$, $C_{d,1}$ and $C_{d,2}$, of the test cell are thus obtained by a low-rate galvanostatic discharge over a short duration [21].

3.2. Analysis

A typical galvanostatic discharge transient for the type HR3 cell at SoC = 1 for 300 s is shown in Fig. 4. The voltage response is exponential in accordance with Eq. (1) and the data are fitted using a Microcal Origin algorithm. The fit is given in the inset from which the impedance data are obtained for the test cell at a particular SoC value, where

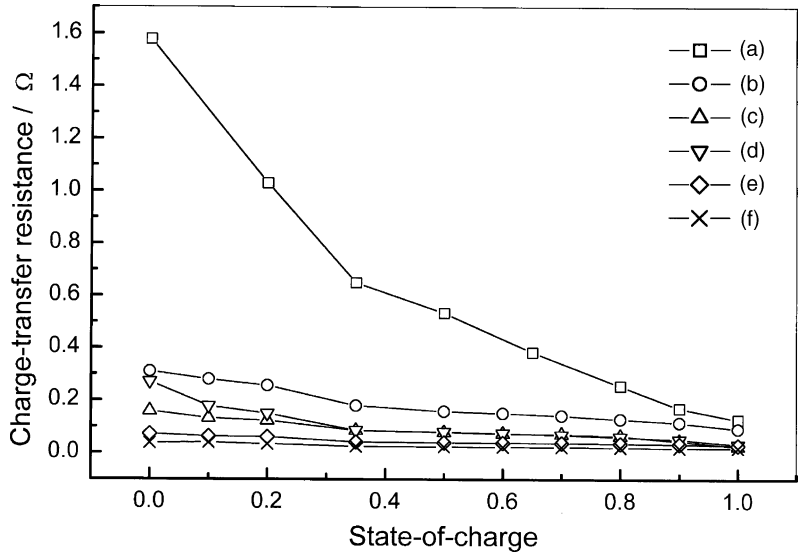

Fig. 5. Charge-transfer resistance as function of SoC for Zn|Zn(OH)$_2$ electrode in silver–zinc cells of type: (a) HR1, (b) HR3, (c) HR5, (d) HR10, (e) HR15, (f) HR40.

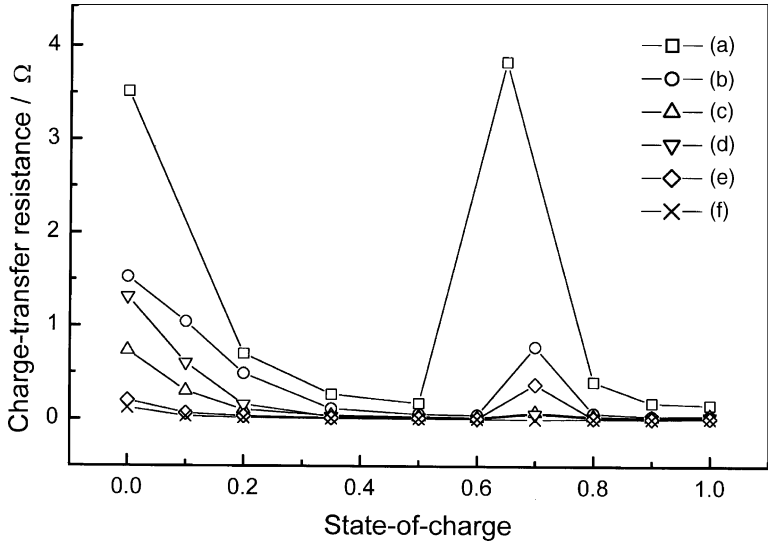

Fig. 6. Charge-transfer resistance as function of SoC for AgO|Ag electrode in silver–zinc cells of type: (a) HR1, (b) HR3, (c) HR5, (d) HR10, (e) HR15, (f) HR40.

$y(0)$ corresponds to the ohmic resistance, $A(1)$ and $A(2)$ are the charge-transfer resistances of the electrodes 1 and 2, respectively, and $t(1)$ and $t(2)$ are the corresponding time constants.

The silver–zinc cells were found to have consistently low ohmic resistance values independent of the size of the cell. Charge-transfer resistance values for the first electrode with its varying SoC are shown in Fig. 5. From the charge-transfer resistance behavior of the first electrode, it is evident that the first electrode is $Zn|Zn(OH)_2$ electrode. An increase in charge-transfer resistance with SoC indicates the conversion of metallic zinc to poorly-conducting zinc hydroxide.

The variation in charge-transfer resistance as a function of SoC for the second electrode shown in Fig. 6 suggest that the second electrode is AgO|Ag. There is a gradual increase in charge-transfer resistance for a change in SoC from 1 to 0.08, followed by an abrupt increase at around SoC = 0.7 which decrease at the same rate as the SoC approach 0.6 followed by a gradual increase towards SoC = 0. This is due to a two-step conversion [2,3,26] of divalent silver oxide to metallic silver through a moderately conducting monovalent silver oxide [27], i.e.

$$2AgO + Zn + H_2O \underset{\text{charge}}{\overset{\text{discharge}}{\rightleftarrows}} Ag_2O + Zn(OH)_2,$$

$$E = 1.86\,\text{V} \quad (\text{Step } 1)$$

$$Ag_2O + Zn + H_2O \underset{\text{charge}}{\overset{\text{discharge}}{\rightleftarrows}} 2Ag + Zn(OH)_2,$$

$$E = 1.60\,\text{V} \quad (\text{Step } 2)$$

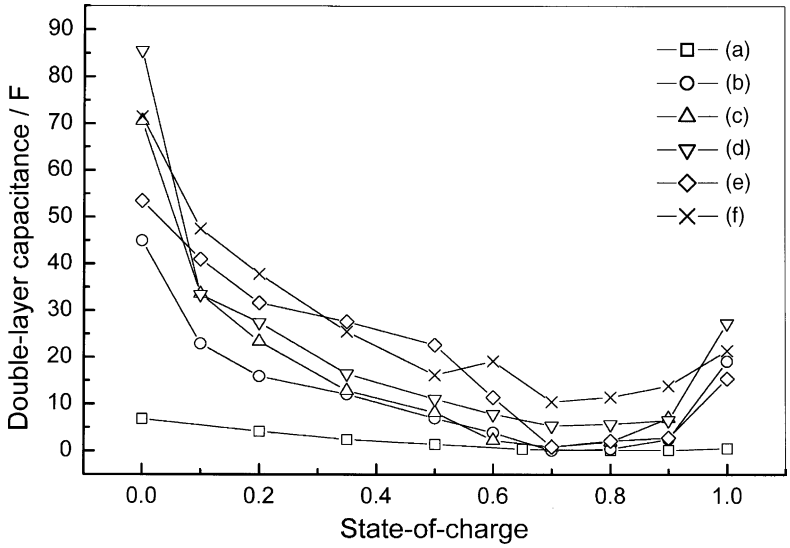

Fig. 7. Double-layer capacitance of $Zn|Zn(OH)_2$ electrode in silver–zinc cells of type (a) HR1, (b) HR3, (c) HR5, (d) HR10, (e) HR15 and (f) HR40 as function of SoC.

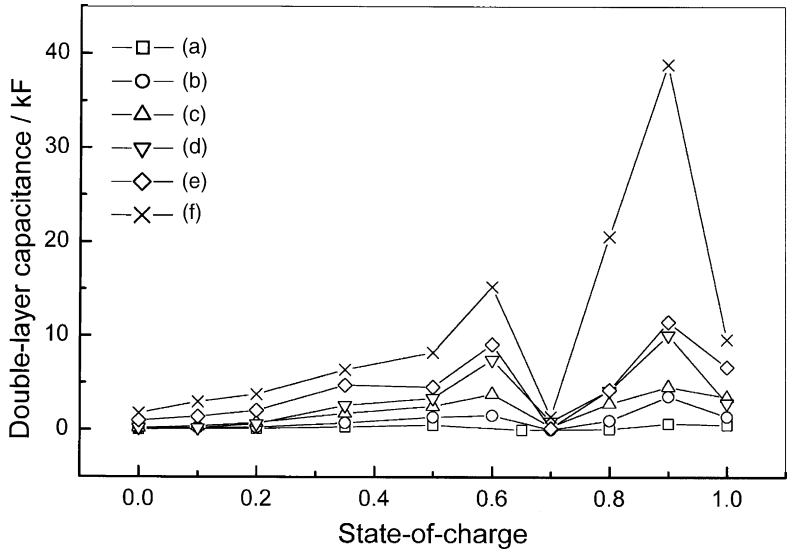

Fig. 8. Double-layer capacitance of AgO|Ag electrode in silver–zinc cells of type (a) HR1, (b) HR3, (c) HR5, (d) HR10, (e) HR15 and (f) HR40 as a function of SoC.

Double-layer capacitance values of the zinc electrode as a function of its SoC are given in Fig. 7. There is a gradual increase with decrease in SoC values, and is due to the conversion of metallic zinc to porous zinc hydroxide. Double-layer capacitance values of silver oxide electrode as a function of SoC are given in Fig. 8, The data show a maximum double-layer capacitance at SoC = 0.9 and a minimum near SoC = 0.7. Subsequent to which the double-layer capacitance increase to 15 kF at SoC = 0.7 followed by a gradual decrease between SoC = 0.6 and 0. It is worth noting that the double-layer capacitance values of AgO|Ag electrodes are about 3 orders higher in magnitude than those of Zn|$Zn(OH)_2$ electrodes.

By contrast, the charge-transfer resistance values of the zinc electrode are higher than those for the silver electrode at all SoC values except for SoC = 0 in silver–zinc cells of type HR5, HR10, HR15 and HR40. Cells of type HR1 and HR3, exhibit higher charge-transfer resistance values for silver electrode than those observed for zinc electrode at SoC = 0.7 and 0. The internal resistance as function of SoC for the cells are given in Fig. 9, and the data suggest that the internal resistance of these cells depends on the size of the cells. It is observed that larger cells have lesser internal resistance. Among the cells studied here, type HR40 cells are found to have the minimum internal resistance and hence can sustain high-drain application.

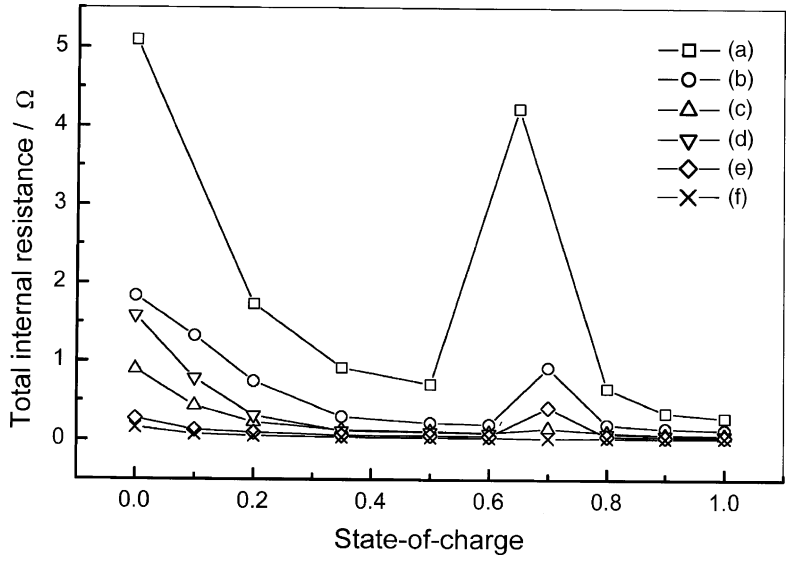

Fig. 9. Internal resistance of silver–zinc cells of type (a) HR1, (b) HR3, (c) HR5, (d) HR10, (e) HR15 and (f) HR40 as a function of SoC.

4. Conclusions

A galvanostatic non-destructive study conducted on alkaline silver–zinc cells of varying capacity suggests that only the cells of type HR5, HR10, HR15 and HR40 with capacities between 10.6 and 58.5 Ah can be used for high-rate discharge applications. These cells also exhibit high Faradaic efficiencies.

Acknowledgements

The authors are grateful to Dr. V. Ganesh Kumar for his invaluable help with this study.

References

[1] A.P. Karpinski, B. Makovetski, S.J. Russell, J.R. Serenyi, D.C. Williams, J. Power Sources 80 (1999) 53.
[2] A. Fleischer, J.J. Lander, Zinc–Silver Oxide Batteries, Wiley, New York, USA, 1971.
[3] U. Falk, A.J. Salkind, Alkaline Storage Batteries, Wiley, New York, USA, 1971.
[4] O. Hasvold, N. Storkersen, J. Power Sources 96 (2001) 252.
[5] J. Skelton, R. Serenyi, J. Power Sources 65 (1997) 39.
[6] A.P. Pavlov, L.K. Grigorieva, S.P. Chizhik, V.K. Stankov, J. Power Sources 62 (1996) 113.
[7] K. Takeda, T. Hattori, J. Electrochem. Soc. 148 (2001) A44.
[8] D.F. Smith, G.R. Graybill, R.K. Grubbs, J.A. Gucinski, J. Power Sources 65 (1997) 47.
[9] D.F. Smith, J.A. Gucinski, J. Power Sources 80 (1999) 66.
[10] H.L. Lewis, T. Danko, A. Himy, W. Johnson, J. Power Sources 80 (1999) 61.
[11] H. Lewis, P. Jackson, A. Salkind, T. Danko, R. Bell, J. Power Sources 96 (2001) 128.
[12] D.F. Smith, C. Brown, J. Power Sources 96 (2001) 121.
[13] X. Jin, J. Lu, Y. Xia, P. Liu, H. Tong, J. Power Sources 102 (2001) 124.
[14] J. McBreen, E. Gannon, J. Power Sources 15 (1985) 169.
[15] F.R. McLarnon, E.J. Cairns, J. Electrochem. Soc 138 (1991) 645.
[16] J. McBreen, J. Power Sources 51 (1994) 37.
[17] J. Jindra, J. Power Sources 6 (1997) 15.
[18] K. Bass, P.J. Mitchell, G.D. Wilcox, J. Smith, J. Power Sources 35 (1991) 333.
[19] D. Linden, T.B. Reddy (Eds.), Hand Book of Batteries, third ed., McGraw-Hill, New York, USA, 2002.
[20] H.A. Frank, W.L. Long, A.A. Uchiyama, J. Electrochem. Soc 123 (1976) 1.
[21] A.K. Shukla, V. Ganesh Kumar, N. Munichandrian, T.S. Srinath, J. Power Sources 74 (1998) 234.
[22] V. Ganesh Kumar, N. Munichandraiah, A.K. Shukla, J. Appl. Electrochem. 27 (1997) 43.
[23] V. Ganesh Kumar, N. Munichandraiah, A.K. Shukla, J. Power Sources 63 (1996) 203.
[24] S.A. Ilangovan, Ph.D Thesis, Indian Institute of Science, Bangalore, 1991.
[25] S.A. Ilangovan, S. Sathyanarayana, J. Appl. Electrochem. 22 (1992) 456.
[26] X. Jin, J. Lu, J. Power Sources 104 (2002) 253.
[27] A. Tvarusko, J. Electrochem. Soc. 115 (1968) 1105.